

# Location, Dissection, and Analysis of the Murine Stellate Ganglion

Katharina Scherschel<sup>1,2,3</sup>, Hanna Bräuninger<sup>3,4</sup>, Klara Glufke<sup>2</sup>, Christiane Jungen<sup>2,4,5</sup>, Nikolaj Klöcker<sup>3</sup>, Christian Meyer<sup>1,2,3</sup>

<sup>1</sup> Division of Cardiology, EVK Düsseldorf, cNEP, cardiac Neuro- and Electrophysiology Research Consortium <sup>2</sup> DZHK (German Centre for Cardiovascular Research) <sup>3</sup> Institute of Neural and Sensory Physiology, Medical Faculty, Heinrich Heine University Düsseldorf <sup>4</sup> Clinic for Cardiology, University Heart & Vascular Centre, University Hospital Hamburg-Eppendorf <sup>5</sup> Department of Cardiology, Leiden University Medical Center

## Corresponding Author

Christian Meyer

christian.meyer@evk-duesseldorf.de

## Citation

Scherchel, K., Bräuninger, H., Glufke, K., Jungen, C., Klöcker, N., Meyer, C. Location, Dissection, and Analysis of the Murine Stellate Ganglion. *J. Vis. Exp.* (), e62026, doi:10.3791/62026 (2020).

## Date Published

December 1, 2020

## DOI

10.3791/62026

## URL

joVE.com/t/62026

## Abstract

The autonomic nervous system is a substantial driver of cardiac electrophysiology. Especially, the role of its sympathetic branch is an ongoing matter of investigation in the pathophysiology of ventricular arrhythmias (VA). Neurons in the stellate ganglia (SG)-bilateral star-shaped structures of the sympathetic chain-are an important component of the sympathetic infrastructure. The SG are a recognized target for the treatment via cardiac sympathetic denervation in patients with therapy-refractory VA. While neuronal remodeling and glial activation in the SG have been described in patients with VA, the underlying cellular and molecular processes that potentially precede the onset of arrhythmia are only insufficiently understood and should be elucidated to improve autonomic modulation. Mouse models allow us to study sympathetic neuronal remodeling, but identification of the murine SG is challenging for the inexperienced investigator. Thus, in-depth cellular and molecular biological studies of the murine SG are lacking for many common cardiac diseases. Here, we describe a basic repertoire for dissecting and studying the SG in adult mice for analyses at RNA level (RNA isolation for gene expression analyses, in situ hybridization), protein level (immunofluorescent whole mount staining), and cellular level (basic morphology, cell size measurement). We present potential solutions to overcome challenges in the preparation technique, and how to improve staining via quenching of autofluorescence. This allows for the visualization of neurons as well as glial cells via established markers in order to determine cell composition and remodeling processes. The methods presented here allow characterizing the SG to gain further information on autonomic dysfunction in mice prone to VA and can be complemented by additional techniques investigating neuronal and glial components of the autonomic nervous system in the heart.

## Introduction

The cardiac autonomic nervous system is a tightly regulated equilibrium of sympathetic, parasympathetic, and sensory components that allows the heart to adapt to environmental changes with the appropriate physiological response<sup>1,2</sup>. Disturbances in this equilibrium, for example, an increase of sympathetic activity, have been established as a key driver for the onset as well as maintenance of ventricular arrhythmias (VA)<sup>3,4</sup>. Therefore, autonomic modulation, achieved via pharmacological reduction of sympathetic activity with beta-blockers, has been a cornerstone in the treatment of patients with VA for decades<sup>5,6</sup>. But despite pharmacological and catheter-based interventions, a relevant number of patients still suffers from recurrent VA<sup>7</sup>.

Sympathetic input to the heart is mostly mediated via neuronal cell bodies in the stellate ganglia (SG), bilateral star-shaped structures of the sympathetic chain, which relay information via numerous intrathoracic nerves from the brainstem to the heart<sup>8,9,10</sup>. Nerve sprouting from the SG after injury is associated with VA and sudden cardiac death<sup>11,12</sup>, emphasizing the SG as a target for autonomic modulation<sup>13,14</sup>. A reduction of sympathetic input to the heart can be achieved temporarily via percutaneous injection of local anesthetics or permanently by partial removal of the SG via video-assisted thoracoscopy<sup>15,16</sup>. Cardiac sympathetic denervation presents an option for patients with therapy-refractory VA with promising results<sup>14,16,17</sup>. We have learned from explanted SG of these patients that neuronal and neurochemical remodeling, neuro-inflammation and glial activation are hallmarks of sympathetic remodeling that might contribute or aggravate autonomic dysfunction<sup>18,19</sup>. Still, the underlying cellular and molecular processes in these neurons remain obscure to date, for

example, the role of neuronal transdifferentiation into a cholinergic phenotype<sup>20,21</sup>. Experimental studies present novel approaches to treat VA, for example, the reduction of sympathetic nerve activity via optogenetics<sup>22</sup>, but in-depth characterization of the SG is still lacking in many cardiac pathologies that go in hand with VA. Mouse models mimicking these pathologies allow to study neuronal remodeling that potentially precedes the onset of arrhythmias<sup>12,23</sup>. These can be completed by further morphological and functional analyses for autonomic characterization of the heart and the nervous system. In the present protocol, we provide a basic repertoire of methods allowing to dissect and characterize the murine SG to improve the understanding of VA.

## Protocol

All procedures involving animals were approved by the Animal Care and Use Committee of the State of Hamburg (ORG870, 959) and conform to the National Institutes of Health's Guide for the Care and Use of Laboratory Animals (2011). Studies were performed using male and female (aged 10-24 weeks) C57BL/6 mice (stock number 000664, Jackson Laboratories) and mice homozygous (db/db) or heterozygous (db/het; control) for the diabetes spontaneous mutation (Lepr<sup>db</sup>; BKS.Cg-Dock7<sup>m+/+</sup> Lepr<sup>db</sup> / J, stock number 000642, Jackson Laboratories). The authors have used the protocols at hand without variations for mice aged up to 60 weeks.

### 1. Location and dissection of murine stellate ganglia

**NOTE:** Even though descriptions and drawings are mostly available in bigger species, some publications have

previously described the location of the SG in rats<sup>24</sup> and mice<sup>25</sup> using anatomical methods and fluorescent reporter lines, respectively.

1. Prepare 50 mL of ice-cold (3–4 °C) heparinized (20 units/mL, see **Table of Materials**) phosphate-buffered saline (PBS). Perform dissection of the SG at room temperature (RT).
2. Deeply anesthetize mouse by inhalation of 3%–5% isoflurane according to the institutional and local guidelines. Verify adequate anesthesia by loss of pedal withdrawal reflex. Decapitate mice or perform cervical dislocation.  
**NOTE:** Incorrect cervical dislocation can result in breakage of the spine and damage of thoracic vessels leading to bleeding which hinders in the preparation or the severing of the sympathetic chain, so that SG are not in their correct position. Therefore, it is critical to have experienced personnel perform cervical dislocation or decapitate animals in deep sedation.
3. Spray the skin with ethanol and open the thorax with two incisions along the anterior axillary lines using Mayo scissors and narrow pattern forceps. Cut the diaphragm and remove the complete ribcage.
4. Remove the heart-lung package by gripping the aorta and vena cava right above the diaphragm using London forceps and cutting all vessels and connective tissue close to the spine below with the Strabismus scissors.
5. Flush the thorax thoroughly with heparinized PBS using a plastic disposable pipette until all traces of blood are removed.

6. Place the torso under stereomicroscope preparation binoculars and ensure good lighting in the thorax with external light sources.
7. Locate the first rib and the longus colli muscles.  
**NOTE:** The SG are located bilaterally, parallel to the spine at the branch between the first rib and the spine, in a groove lateral to the longus colli muscles<sup>24</sup>. The flat side of the SG is located adjacent to the longus colli muscles. Depending on the preparation, parts of the sympathetic chain might already be visible as white, oblique fibers parallel to the spine. These can be traced along to the SG.
8. Gently use the tip of the Dumont #5/45 forceps to expose the connective tissue lateral to the longus colli muscle.
9. Turn the forceps around by 180° and use the flat side to grip the SG and pull it out with minimal pressure.
10. Repeat with the second SG.
11. Place both SG in a dish (6 cm diameter) filled with cold PBS and inspect with the appropriate magnification. If necessary, remove excess vessels, fat tissue, and larger nerves.  
**NOTE:** Autonomic ganglia are surrounded by a connective tissue capsule consisting of collagen fibers and fibroblasts<sup>26,27</sup>. The permeability of these capsules seems to vary among species, different kind of ganglia<sup>26</sup> and age<sup>28</sup>. Remove as much connective tissue as possible using Dumont #5/45 forceps and, if necessary, spring scissors. Depending on the goal of the experiment, proceed with section 2, 3, or 4 of this protocol.

## 2. Whole mount immunohistochemistry protocol

**NOTE:** This protocol is adapted from cardiac whole mount stainings<sup>4,29</sup>. Perform incubation steps for every single SG

in one well of a 96-well plate and use 100  $\mu$ L (for antibody-containing solutions) to 200  $\mu$ L (for all other solutions) of the solution to ensure complete coverage. Regularly check the coverage and correct immersion of the SG with binoculars. Remove liquids manually with a 200  $\mu$ L pipette with an additional 10  $\mu$ L tip on top of the 200  $\mu$ L tip. This will prevent aspiration of the SG in the pipette tip. Use freshly prepared solutions and sterile liquids to prevent bacterial growth.

1. Fix SG for histology for 2 h at RT in 4% methanol-free paraformaldehyde (PFA)/PBS.
2. Process SG as quickly as possible, but they can be stored for 2-4 weeks at 4-6 °C in PBS with 0.02% (w/v) sodium azide at this point.
3. Prepare Sudan black stock solution (1% Sudan black w/v in 100% ethanol) for reduction of autofluorescence and improvement of signal to background ratio<sup>30</sup>. Dissolve for 2-3 h on a magnetic stirrer at RT.  
**NOTE:** Use the stock solution for a maximum of 6-8 weeks, discard earlier when sedimentation appears.
4. Prepare Sudan black working solution by centrifuging the stock solution for 30 min at full speed (13,000  $\times$  g) to remove debris and diluting the stock in 70% ethanol to a final concentration of 0.25% Sudan black.
5. Treat SG with Dent's bleach to improve antibody permeabilization<sup>31</sup>. Freshly prepare Dent's bleach by mixing methanol (MeOH), hydrogen peroxide solution 30% (w/w) in H<sub>2</sub>O and dimethyl sulfoxide (DMSO) in a ratio of 4:1:1. Add 200  $\mu$ L per SG and place the plate on an orbital shaker for 1 h at RT.
6. Perform a descending MeOH series for rehydration by incubating for 10 min each on an orbital shaker: 100%

MeOH, 75% MeOH/PBS, 50% MeOH/PBS, 25% MeOH/PBS.

7. Perform permeabilization by incubating SG twice for 60 min each in PBS/1% Triton-X-100 at RT.
8. Remove permeabilization solution from the SG and add Sudan black working solution. Incubate for 2 h at RT on an orbital shaker.
9. In the meantime, prepare a blocking solution by adding 5% receptor grade bovine serum albumin (BSA) and 0.1% Triton-X-100 in PBS a 15 mL vessel and let it dissolve on a roller shaker for approximately 5-10 min. Decant through a pre-pleated paper filter to remove debris.
10. Remove Sudan black very carefully by tilting the plate and carefully pipetting from the upright side.  
**NOTE:** It is not possible to see the SG in Sudan black. Use a strong light source and work slowly. From this step on, SG are stained black, enhancing visualization. If any additional connective tissue is seen surrounding SG at this point, remove it using Dumont #5/45 forceps and spring scissors.
11. Add 200  $\mu$ L of PBS/0.1% Triton-X-100 (PBS-T) and wash for 5 min at RT on an orbital shaker.
12. Remove PBS-T by aspirating it with a pipette and repeat 2 times.
13. Remove PBS; add 200  $\mu$ L of blocking solution and incubate at 4 °C overnight on an orbital shaker.
14. On the next day, prepare solutions by adding primary antibodies in the blocking solution. Adapt antibody concentrations from established protocols.

**NOTE:** Include one SG as antibody control without primary antibody (incubated with antigen-preabsorbed antibody or IgG, if available, or blocking buffer).

15. Perform primary antibody incubation for 36-48 h at 4 °C on an orbital shaker. For cell size measurements and staining of sympathetic neurons, use antibodies against tyrosine hydroxylase (see **Table of Materials** for antibody recommendations).

**NOTE:** Place the 96-well plate in a wet chamber (e.g., plastic box lined with ddH<sub>2</sub>O-wetted paper towels) to prevent evaporation at this point.

16. Remove antibody solution carefully and add 200 µL of PBS-T. Place the plate on an orbital shaker for 30 min.

17. Remove PBS-T and repeat the washing step 5 additional times.

18. Prepare the secondary antibody working solution by centrifuging fluorescent Alexa-labeled secondary antibodies for 1 min at full speed (13,000 x g) before usage. Dilute the appropriate secondary antibodies according to the primary antibodies 1:500 in the blocking solution and add to SG. Add 1 µg/mL of bisbenzimidazole H33342 trihydrochloride (Hoechst staining) if nuclear staining is desired. Incubate for 12-24 h at 4 °C on an orbital shaker.

19. Remove the antibody solution carefully and add 200 µL of PBS-T. Place the plate on an orbital shaker for 30 min.

20. Remove PBS-T and repeat the washing step 5 additional times. For the last step, use PBS without Triton.

21. For embedding, spread 50-100 µL of fluorescent mounting medium (see **Table of Materials**) on a glass slide and place under preparation binoculars. Use Dumont #5/45 forceps to pick up SG from the 96-well plate and remove excess liquid by dipping one end on a filter paper (e.g., Whatman drying pad) and place it on the drop.

22. Use Dumont #5/45 forceps to correct positioning with the appropriate magnification.

23. Gently place a glass coverslip (20 mm x 20 mm) next to the SG and slowly descend.

**NOTE:** Using too much mounting medium will result in movement of the SG or tangling of nerves. If that happens, quickly remove the coverslip and repeat steps 2.9-2.21.

24. Let the slides dry in the dark overnight at RT. Storage of the stained specimen is possible for at least 4-6 weeks at 4 °C.

### 3. Whole mount in situ hybridization

**NOTE:** Whole-mount in situ-hybridization of the SG is adapted from the organ of corti<sup>32</sup> and the commercial RNA fluorescence in situ protocol (see **Table of Materials**). Obtain probes for the genes of interest and buffers and solutions from the supplier. All incubation steps are performed at RT, if not mentioned otherwise. Use sterile PBS. If interested in staining several SG in one well, use at least 150 µL of buffers and solutions.

1. Perform dissection of the SG as described in steps 1.1-1.13.
2. Fixate SG for 1 h in 200 µL of 4% MeOH-free PFA/PBS in one well of a 96-well plate placed on an orbital shaker.
3. Wash SG three times for 30 min each in 0.1% Tween-20/PBS on an orbital shaker.
4. Dehydrate SG in MeOH/PBS series by subsequent incubation in 50% MeOH/PBS, 70% MeOH/PBS, and 100% MeOH for 10 min each on an orbital shaker.
5. Store SG at -20 °C in 100% MeOH overnight.
6. The next day, pre-warm the incubator to 40 °C. Check the temperature with a thermometer.

7. Rehydrate SG in reverse MeOH/PBS series (100% MeOH, 70% MeOH/PBS, 50% MeOH/PBS) for 10 min each.
8. Wash SG three times for 5 min each in PBS.
9. In the meantime, start pre-warming the probes by incubation at 40 °C for 10 min, followed by cooling for 10 min.
10. Incubate SG in 200 µL of Protease III for 15 min.
11. Optional: Perform Sudan black treatment to quench autofluorescence according to sections 2.3, 2.7, and 2.8 of this protocol if subsequent immunofluorescence staining is planned.
12. Wash SG in 200 µL of 0.1% Tween-20/PBS 3x for 5 min each on an orbital shaker.
13. Optional: If co-staining with several probes is desired, dilute Channel-2 (50x) and Channel-3 probe (50x) in Channel-1 probe (1x).
14. Cover SG with 100 µL of probe for the gene of interest and incubate overnight at 40 °C with slight agitation. Place the 96-well plate in a wet chamber at 40 °C for all incubation steps.  
**NOTE:** Include one SG as negative control, using a probe against a bacterial gene (e.g., dihydro-dipicolinate reductase, *DapB*) to check for non-specific binding of amplification reagents in later steps.
15. Wash SG in supplied washing buffer 3x for 15 min each on an orbital shaker.
16. Pre-warm Amp1-3, HRP-C1, and HRP-Blocker to RT. If co-staining with Channel-2 and/or Channel-2 probe is desired, pre-warm HRP-C2 and HRP-C3.
17. Re-fix SG for 10 min at RT in 4% PFA/PBS on an orbital shaker.
18. Wash SG in 200 µL of supplied washing buffer 3x for 5 min each on an orbital shaker at RT.
19. For amplification, incubate SG with 100 µL of Amp1 for 35 min at 40 °C on an orbital shaker.
20. Carefully remove any liquid and wash SG in 200 µL of supplied washing buffer 3x for 5 min each at RT on an orbital shaker.
21. Incubate SG with 100 µL of Amp2 for 35 min at 40 °C on an orbital shaker.
22. Repeat step 3.18.
23. Incubate SG with 100 µL of Amp3 for 20 min at 40 °C on an orbital shaker.
24. Repeat step 3.18.
25. Incubate SG with 100 µL of supplied Multiplex FL v2 HRP-C1 for 20 min at 40 °C on an orbital shaker.
26. Repeat step 3.18.
27. Prepare Opal-conjugated secondary antibody 1:1,000 in 200 µL of supplied TSA-buffer and incubate SG for 35 min at 40 °C on an orbital shaker. Protect from light during incubation and from this step on.
28. Repeat step 3.18.
29. Incubate SG in 100 µL of supplied Multiplex FL v2 HRP-blocker for 15 min at 40 °C on an orbital shaker.
30. Repeat step 3.18.
31. Optional: For co-staining with Channel-2 probe, repeat steps 3.25-3.30 with supplied Multiplex FL v2 HRP-C2.
32. Optional: For co-staining with Channel-3 probe, repeat steps 3.25-3.30 with supplied Multiplex FL v2 HRP-C3.
33. In case of subsequent immunofluorescent staining, perform steps 2.14-2.25 of this protocol.



34. Incubate in 1% BSA/PBS for 30 min on an orbital shaker.
35. Incubate SG for 30 min in 1 µg/mL of bisbenzimidazole H33342 trihydrochloride (Hoechst staining) in 1% BSA/PBS if nuclear staining is desired and/or add Alexa-coupled wheat germ agglutinin (WGA, 1:500) on an orbital shaker.
36. Repeat step 3.18.
37. Embed as described in steps 2.19-2.22.

#### 4. Imaging and analyses of murine stellate ganglia

1. Perform confocal microscopy of embedded SG in the local imaging facility.
2. If cell size measurements are required, image SG stained for tyrosine hydroxylase (see **Table of Materials**) at 200x magnification and take 4-6 random images from every SG.
3. Analyze images using ImageJ<sup>33</sup> software to estimate cell size (e.g., with a pen table, see **Table of Materials**). Use **Free Hand Selection**, circle each cell and click on **Analyze | Measure** to obtain cell area. Be careful to include only intact, fully visible cells that are located well within the SG.
4. Using this method, perform measurement of approximately 100 cells per SG.
5. Have a blinded investigator perform steps 4.2-4.3 if you want to compare SG from different mice. Use a frequency distribution in statistical software to visualize size differences between groups<sup>34</sup>.

#### 5. Molecular analyses of murine stellate ganglia

**NOTE:** Include controls depending on your experimental design. This could be SG with different genotypes and

disease background and/or other autonomic ganglia, such as the sympathetic superior cervical ganglion (located in the neck area, see detailed description in Ziegler et al.<sup>35</sup>) or parasympathetic ganglia (such as intracardiac ganglia, see Jungen et al.<sup>4</sup>).

1. Prepare a 2 mL tube with 500 µL of phenol/guanidine thiocyanate solution (e.g., Qiazol) per animal and have liquid nitrogen ready for shock-freezing or consider commercial solutions for protection of RNA (optional, see **Table of Materials**)<sup>36</sup>. Work quickly for RNA isolation.
2. Perform dissection of the SG as described in steps 1.1-1.13.
3. Immediately immerse both SG directly in one tube with phenol/guanidine thiocyanate solution and shock-frost tube in liquid nitrogen.
4. Store at -80 °C until further processing.
5. For tissue lysis, let tubes with SG thaw until phenol/guanidine thiocyanate solution is liquified and add two 7 mm stainless steel beads. Cool down the metal parts of tissue homogenizer (ball or mixer mill, e.g., Tissue Lyser II) on dry ice and centrifuge to 4 °C.
6. Centrifuge tubes at 500 x g for 1 min at 4 °C so that SG are at the bottom of the tube.
7. Put tubes into the metal parts of the Tissue Lyser and lyse for 1 min at 20 Hz.
8. Repeat steps 5.6 and 5.7 up to 5 times until no intact tissue is detectable.
9. Transfer the liquid into a fresh 1.5 mL tube.
10. Perform RNA isolation with a column-based RNA isolation kit (e.g., miRNeasy mini kit) according to the manufacturer's instructions.

11. Elute RNA in 20  $\mu$ L of RNase-free water and measure concentration using a spectrophotometer.

**NOTE:** To exclude contamination of the purified RNA with genomic DNA, we propose performing a polymerase chain reaction with genomic primers and 1  $\mu$ L of RNA as template, instead minus reverse transcriptase control. This will save a significant amount of RNA. If RNA is contaminated, use exon-intron boundary primers or intron flanking primers for subsequent quantitative real-time polymerase chain reaction.

12. Use 250 ng SG RNA to perform cDNA synthesis and use established protocols. Here a high-capacity cDNA reverse transcription kit was used according to the manufacturer's instructions.

13. Dilute to a final concentration of 2.5 ng/ $\mu$ L of cDNA and perform quantitative real-time polymerase chain reaction with the appropriate probes according to the established protocols. Here TaqMan Assay (see **Table of Materials**) was performed using 10 ng cDNA per reaction.

**NOTE:** Perform no-template control for every gene to exclude false positive results.

14. Normalize gene expression of your gene of interest on a house keeping gene (e.g., *Cdkn1b*) to compare relative gene expression between different groups of SG.

## Representative Results

**Figure 1** visualizes how to identify and dissect the SG.

**Figure 1A** shows a schematic drawing of the location, while

**Figure 1B** presents the view of the thorax after removal of the heart-lung-package. The left and right longus colli muscles medial from the SG and the rib cage are important landmarks for orientation. Dissection is performed along the dotted lines between muscles and the first rib. The SG and the sympathetic chain become visible as white structures (**Figure**

**1C**). **Figure 1D** shows a magnification of the region between the left longus colli muscle and the first rib, where the left SG is located. Morphology of the SG differs between individuals. It often consists of a fusion of the inferior cervical and the first to the third thoracic ganglia<sup>24</sup>. Some variety that the experimenter can expect in murine SG is depicted in **Figure 1E,F**, where left and right SG of five male C57Bl6 wild type mice are photographed.

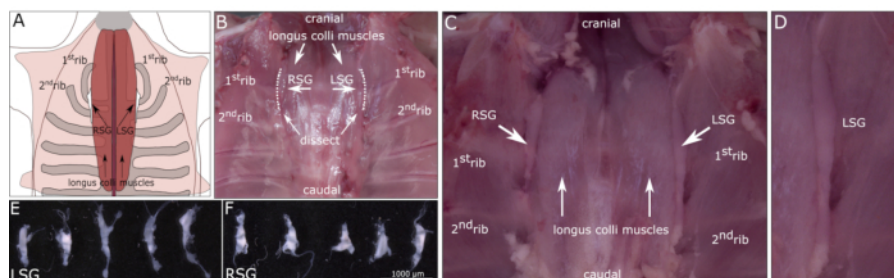


The gross anatomic overview, cellular and subcellular analyses of cells in the SG innervating the heart can be performed by whole mount techniques on protein and RNA level. An overview of a SG is presented in **Figure 2**. Myocardial sympathetic fibers originate from cell bodies in the SG. These are visualized by staining with an antibody against tyrosine hydroxylase (TH). TH-expressing neuronal somata are surrounded by nerve fibers staining positive for choline acetyltransferase (ChAT). These are most likely presynaptic fibers<sup>37,38</sup>. An exemplary magnification from TH and ChAT co-labeling is presented in **Figure 2A**. Glial cells surrounding neuronal cell bodies can be visualized by staining for S100B. This is depicted in **Figure 2B** in combination with the neural marker PGP9.5. **Figure 2C-F** show exemplary analyses to study the SG on a subcellular level, using whole mount in situ hybridization and immunofluorescent co-staining. The protein TH (**Figure 2C**, red) and mRNA molecules of *Tubb3* (**Figure 2D**, white) are expressed in large neuronal cell bodies, while mRNA of *S100b* (**Figure 2E**, green) is also detectable in surrounding glia cells. In the merge (**Figure 2F**), it is visible that some neurons are negative for TH but express *Tubb3*, while *S100b* mRNAs can also be detected in surrounding cells, as depicted in the magnification in **Figure 2G**.

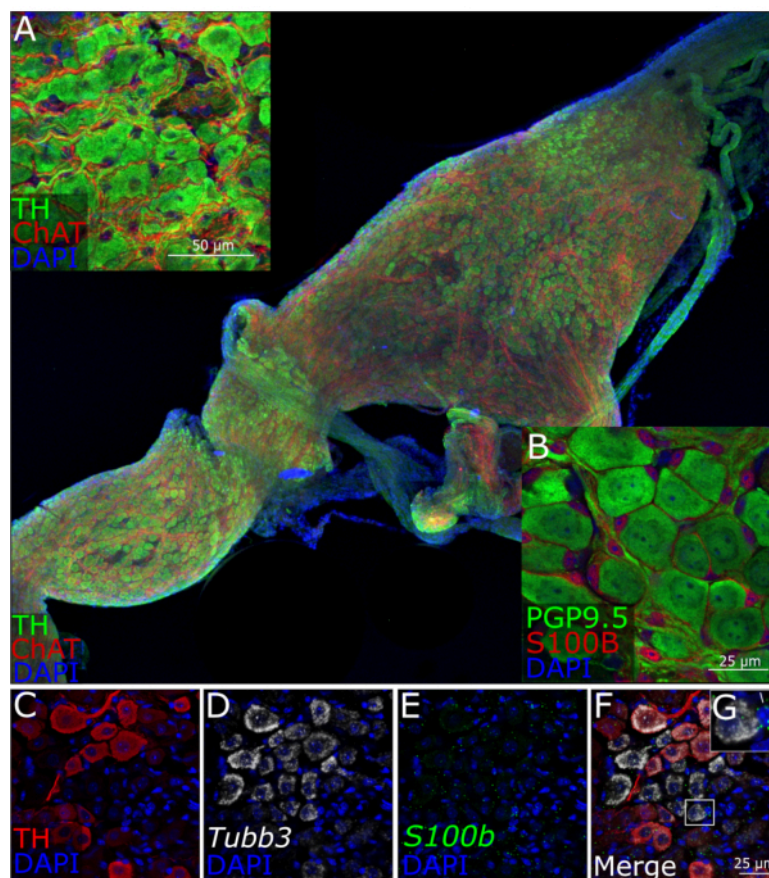
**Figure 3** presents potential quantitative analyses and pitfalls for studying the murine SG. Images from TH-stained SG (**Figure 3A**) can be used for cell size measurements as was performed exemplary for a mouse model of diabetes. Neuronal somata from control (db/het) SG were  $388.8 \pm 123.8 \mu\text{m}^2$  vs. in diabetic SG (db/db)  $407.33 \pm 139.6 \mu\text{m}^2$  (**Figure 3B**,  $n = 2$  SG, 100 cells per SG per genotype,  $P = 0.348$ , data were compared using Mann-Whitney test). **Figure 3C** shows the expression of genes from different cell types of the SG ( $n = 6-7$ ). Pooling of both SG from one animal allows gene expression measurements of approximately 24 assays (12 genes in duplicates). We typically normalize samples for *Cdkn1b* (detected at Ct values of  $25.4 \pm 0.97$ ) as well as the neuronal marker *Neun/Rbfox3* ( $32.5 \pm 0.7$ ) if it is necessary to account for other cell types and neuronal purity of the dissection. Genes that we found useful for characterizing molecular processes in the SG include the sympathetic gene *Th* ( $22.4 \pm 1.6$ ), *Chat*, which could indicate cholinergic transdifferentiation (expressed at Ct values of  $30.8 \pm 1.3$ ) and *Gap43*, a marker for neuronal sprouting (detectable at Ct values of  $22.4 \pm 1.4$ ). Genes expressed in non-neuronal cell type include *S100b* (for glial cells,  $27.3 \pm 1.2$ ), *Ki-67* (for proliferating cells,  $33.0 \pm 1.6$ ) and *Cd45* (for immune cells,  $30.2 \pm 1.1$ ).

The SG is surrounded by a capsule of connective tissue<sup>26</sup>, visualized via hematoxylin and eosin staining in **Figure 3D,E**. Occasionally, we observed inconsistencies in antibody-based staining as demonstrated in **Figure 3F**, most likely due to incomplete removal of the capsule. While ChAT and TH staining are only detectable in some parts of the SG, nuclei counterstained with DAPI are detectable throughout. The dotted line in the merged image separates successful staining (right of the line) from unsuccessful staining (left of the line).

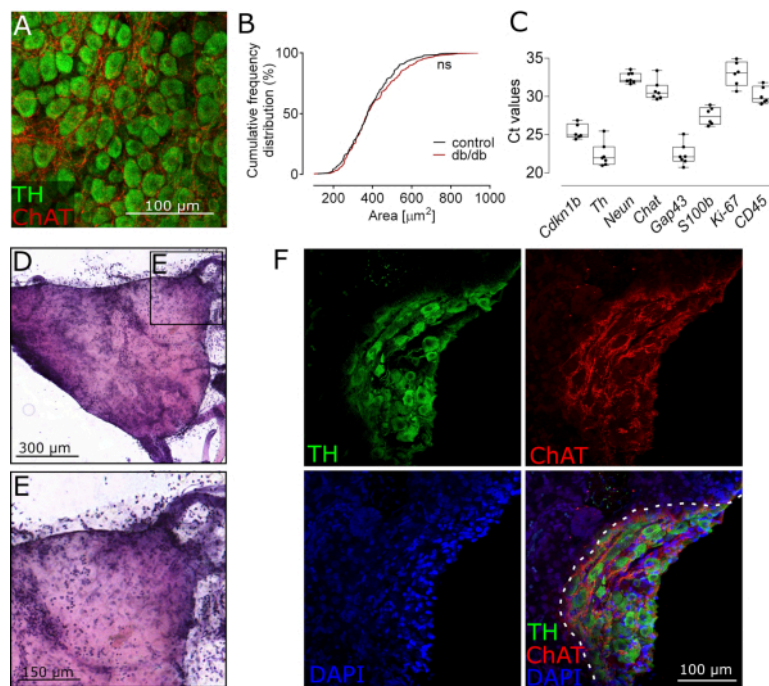
Data are presented as mean  $\pm$  standard deviation. Statistical significance was defined as a P value of  $<0.05$ ; statistical analysis was performed using commercial software.



**Figure 1: Location, dissection, and morphology of the murine stellate ganglia.** (A) Schematic drawing of the location of the stellate ganglia (SG). (B) View into the thorax after removal of the heart-lung package. It is important to note that the SG are not immediately visible most of the time. The longus colli muscles are located lateral from the spine. The SG are located lateral from the muscles at the junction with the first rib. Carefully dissect lateral to the muscles (area marked by dotted line) to uncover the ganglia. After dissection, ganglia (left and right, LSG and RSG, respectively) and the sympathetic chain can be made out as white, long structures. (C) An exemplary dissection showing the ganglia and anatomical landmarks. (D) Magnification of the LSG. (E) LSG and (F) RSG from wild type, male C57Bl6 mice (16 weeks) were dissected and photographed to show the variations in morphology and size. Scale bar represents 1,000  $\mu\text{m}$ . [Please click here to view a larger version of this figure.](#)





**Figure 2: Visualization of different cell types in murine stellate ganglia via whole mount immunohistochemistry and in situ hybridization.** (A) Gross overview of a murine stellate ganglion (SG) stained for the sympathetic marker tyrosine hydroxylase (TH) and choline acetyltransferase (ChAT). The magnification shows TH-positive cell bodies and the presence of ChAT-positive, most likely presynaptic, nerve fibers surrounding neuronal somata. (B) Glial cells ensheathing neuronal cell bodies can be visualized by staining for S100B, here in combination with the neuronal marker PGP9.5. (C,D,E,F) Microscopic images from one SG stained whole mount via a combination of immunohistochemistry for TH (red) and in situ hybridization for *Tubb3* (D, white) and *S100b* (E, green). Nuclei are counterstained with DAPI (blue). (F) The merge shows that not all neuronal (*Tubb3*-positive) cells are TH positive. *S100b* mRNAs can be detected within neuronal somata, but also surrounding cells, as marked by an arrow in the magnification in (G). [Please click here to view a larger version of this figure.](#)



**Figure 3: Potential quantitative analyses and pitfalls.** (A) Images from Tyrosine-hydroxylase (TH)-stained SG can be used for cell size measurements using ImageJ. (B) This was performed in a mouse model of diabetes (100 cells per SG,  $n = 2$  SG per genotype, data was compared using Mann-Whitney test). (C) Exemplary genes expressed in the SG that might be useful for characterizing molecular processes. *Cdkn1b* as well as the neuronal marker *Neun/Rbfox3* (to account for the presence of other cell types) can be used for normalization. Tyrosine hydroxylase (*Th*) serves as a sympathetic marker, choline acetyltransferase (*Chat*) for cholinergic transdifferentiation, *Gap43* for neuronal sprouting. Genes expressed in non-neuronal cell types include *S100b* (glial cells), *Ki-67* (proliferating cells) and *Cd45* (immune cells). (D) Hematoxylin and eosin staining of a formalin-fixed SG visualizes connective tissue and cells on top of the SG. (E) Magnification from the boxed area. (F) On some occasions, we observed failure in antibody-based staining, most likely due to incomplete removal of the capsule. While ChAT (red) and TH (green) staining are only detectable in some parts of the SG, nuclei counterstained with DAPI (dark blue) are detectable throughout. The dotted line in the merged image separates successful staining (right of the line) from unsuccessful staining (left of the line). [Please click here to view a larger version of this figure.](#)

## Discussion

The understanding of cellular and molecular processes in neurons and glial cells of the sympathetic nervous system that precede the onset of VA is of high interest, as sudden cardiac arrest remains the most common cause of death

worldwide<sup>5</sup>. Therefore, in the current manuscript, we provide a basic repertoire of methods to identify the murine SC  key element within this network  and perform subsequent analyses on RNA, protein, and cellular level.



One challenge of the murine SG is its size and the limited number of cells<sup>39</sup>. Due to this, different animal models, such as rats<sup>40</sup>, dogs<sup>22</sup>, and pigs<sup>41</sup> are used for studies on the SG. Still, there is a variety of well-established disease models for cardiac phenotypes available in mice and some of these have already been characterized in different aspects of cardiac innervation and arrhythmia, such as models for diabetes<sup>23</sup>, myocardial infarction<sup>42</sup>, or myocarditis<sup>43</sup>. Therefore, further studies of the murine SG are warranted to further characterize autonomic dysfunction in the light of VA. These can be completed by other approaches to study innervation of the murine heart as functional experiments<sup>4,23,44</sup> including in-vivo stimulation of the SG<sup>23</sup>.

Due to its small size and its location within the thoracic cavity<sup>24</sup>, manipulation of the murine SG in vivo is challenging, although it has been performed successfully<sup>23</sup>. For this reason, some studies therefore focus on the superior cervical ganglia, which are located more accessibly in the neck, upstream of the SG in the sympathetic chain behind the carotid bifurcation into internal and external carotid arteries<sup>24,35</sup>. Cardiac denervation via removal of the superior cervical ganglia has been shown to attenuate myocardial inflammation, hypertrophy, and cardiac dysfunction after myocardial infarction<sup>35</sup>. However, it is important to note that the superior cervical ganglia innervate different regions of the heart, most prominently the anterior side<sup>45</sup>. In addition, a recent in-depth literature review came to the conclusion that the role of cervical ganglia on sympathetic innervation of the heart remains unclear in humans<sup>46</sup>. This highlights the importance of characterizing the SG for studies of cardiac sympathetic innervation.

It is important to note that the heart is not the only target of the SG. Among others, lungs<sup>47</sup> and sweat glands in the

forepaw<sup>48</sup> are also innervated from fibers originating in the SG, the latter are an exception to sympathetic physiology as they express choline acetyltransferase<sup>37</sup>. Temporary blockade of the SG is studied with regard to inflammatory processes in acute lung injury<sup>49</sup> or for treatment of hot flushes and sleep dysfunction<sup>50</sup>; therefore, the protocols at hand might offer a repertoire for mechanistic questions in these fields. When focusing on cardiac disease models, it should be kept in mind for interpretation of results that cardiac neurons cannot be differentiated by morphology or electrophysiological properties from non-cardiac neurons<sup>51</sup>. This can be achieved by retrograde tracing, thereby the location of neurons projecting to the heart was shown to be located in the cranio-medial parts of the SG<sup>52</sup>.

Additionally, it is important to note that besides different types of neurons, sympathetic ganglia are made up of ensheathing glia, so-called satellite glial cells or satellite cells marked by expression of the glial marker S100B<sup>53</sup>. While little is known about the role of these cells in cardiovascular pathologies, glial activation and expression of the glial fibrillary acidic protein (GFAP) has been described in SG from patients with arrhythmias<sup>18</sup>.

Some pitfalls should be kept in mind with the presented methods: we observed inconsistencies in antibody-based staining at some occasions and hypothesized that incomplete removal of the connective tissue capsule ensheathing the SG might be at fault, as they have been described to vary in permeability among different types of ganglia<sup>26</sup>. Mechanical removal of the capsule using fine forceps has been described in the superior cervical ganglion of rats up to postnatal day 10<sup>28</sup> and desheathing is mentioned in literature for adult rat SG<sup>54,55</sup> and mice<sup>56</sup>. Removal of the SG capsule might vary between age<sup>28</sup> and  due to size differences .



species. In our experience, fresh dissection, removal of as much connective tissue as possible using fine forceps and thorough permeabilization as described in the protocol at hand, are important factors for successful staining. Regarding quantitative real-time PCR, quick work and efficient lysis are essential. Pooling both SGs from one animal reliably allowed for the analysis of up to 12 different genes (when performing duplicates).

Even though function and gross anatomy of SG has been studied for decades now and every single cardiomyocyte is innervated by sympathetic fibers<sup>46</sup>, many open questions remain. For example, it remains unclear, why sympathetic neurons of the SG transdifferentiate transiently to a cholinergic phenotype in ischemic<sup>21</sup> and non-ischemic heart failure, in animal models as well as in patients<sup>20</sup>. Recently, our group described a role of S100B-positive glial cells, which are also present in the murine SG, on nerve sprouting in the cardiac nervous system<sup>29</sup>. Whether these cells are relevant for sympathetic nerve sprouting after injury associated with VA<sup>11,12</sup>, needs to be elucidated in future studies. Importantly, innovative approaches, such as optogenetics<sup>52</sup> and transcriptome analyses<sup>36</sup> can complement established methods such as neuronal tracing in order to deepen the understanding of the sympathetic nervous system and its role on cardiac electrophysiology.

In conclusion, this repertoire allows the inexperienced investigator to perform a basic characterization of the SG in murine models of cardiac pathologies. We hope that this will stimulate the usage, combination, and creation of novel methods. This might help to increase the understanding of the underlying cellular and molecular processes in sympathetic neurons that might be responsible for the onset and maintenance of VA.

## Disclosures

The authors have nothing to disclose.

## Acknowledgments

The authors would like to thank Hartwig Wieboldt for his excellent technical assistance, and the UKE Microscopy Imaging Facility (Umif) of the University Medical Center Hamburg-Eppendorf for providing microscopes and support. This research was funded by the DZHK (German Centre for Cardiovascular Research) [FKZ 81Z4710141].

## References

1. Goldberger, J. J., Arora, R., Buckley, U., Shivkumar, K. Autonomic nervous system dysfunction: JACC focus seminar. *Journal of the American College of Cardiology*. **73** (10), 1189-1206 (2019).
2. Jänig, W. Neurocardiology: a neurobiologist's perspective. *The Journal of Physiology*. **594** (14), 3955-3962 (2016).
3. Meng, L., Shivkumar, K., Ajijola, O. Autonomic Regulation and Ventricular Arrhythmias. *Current Treatment Options in Cardiovascular Medicine*. **20** (5) (2018).
4. Jungen, C. et al. Disruption of cardiac cholinergic neurons enhances susceptibility to ventricular arrhythmias. *Nature Communications*. **8**, 14155 (2017).
5. Al-Khatib, S.M. et al. 2017 AHA/ACC/HRS Guideline for management of patients with ventricular arrhythmias and the prevention of sudden cardiac death. *Circulation*. **138** (13), e272-e391 (2018).
6. Yusuf, S., Wittes, J., Friedman, L. Overview of results of randomized clinical trials in heart disease: I. treatments following myocardial infarction. *JAMA: The Journal of*



- the American Medical Association*. **260** (14), 2088-2093 (1988).
7. Sapp, J. L. et al. Ventricular tachycardia ablation versus escalation of antiarrhythmic drugs. *New England Journal of Medicine*. **375** (2), 111-121 (2016).
8. Yasunaga, K., Nosaka, S. Cardiac sympathetic nerves in rats: Anatomical and functional features. *The Japanese Journal of Physiology*. **29** (6) (1979).
9. Pardini, B. J., Lund, D. D., Schmid, P. G. Organization of the sympathetic postganglionic innervation of the rat heart. *Journal of the Autonomic Nervous System*. **28** (3), 193-201 (1989).
10. Meyer, C., Scherschel, K. Ventricular tachycardia in ischemic heart disease: The sympathetic heart and its scars. *American Journal of Physiology - Heart and Circulatory Physiology*. **312** (3), H549-H551 (2017).
11. Cao, J. M. et al. Relationship between regional cardiac hyperinnervation and ventricular arrhythmia. *Circulation*. **101** (16), 1960-1969 (2000).
12. Ren, C. et al. Nerve sprouting suppresses myocardial Ito and IK1 channels and increases severity to ventricular fibrillation in rat. *Autonomic Neuroscience: Basic and Clinical*. **144** (1-2), 22-29 (2008).
13. Zipes, D.P. et al. Treatment of ventricular arrhythmia by permanent atrial pacemaker and cardiac sympathectomy. *Annals of Internal Medicine*. **68** (3), 591-597 (1968).
14. Kusumoto, F. M. et al. Systematic review for the 2017 AHA/ACC/HRS guideline for management of patients with ventricular arrhythmias and the prevention of sudden cardiac death. *Circulation*. **138** (13) (2018).
15. Cronin, E. M. et al. 2019 HRS/EHRA/APHRS/LAQRS Expert Consensus Statement on Catheter Ablation of Ventricular Arrhythmias: Executive Summary. *Heart Rhythm*. (2019).
16. Vaseghi, M. et al. Cardiac sympathetic denervation in patients with refractory ventricular arrhythmias or electrical storm: Intermediate and long-term follow-up. *Heart Rhythm*. **11** (3), 360-366 (2014).
17. Vaseghi, M. et al. Cardiac sympathetic denervation for refractory ventricular arrhythmias. *Journal of the American College of Cardiology*. **69** (25), 3070-3080 (2017).
18. Ajijola, O. A. et al. Inflammation, oxidative stress, and glial cell activation characterize stellate ganglia from humans with electrical storm. *JCI insight*. **2** (18), 1-11 (2017).
19. Rizzo, S. et al. T-cell-mediated inflammatory activity in the stellate ganglia of patients with ion-channel disease and severe ventricular arrhythmias. *Circulation: Arrhythmia and Electrophysiology*. **7** (2), 224-229 (2014).
20. Kanazawa, H. et al. Heart failure causes cholinergic transdifferentiation of cardiac sympathetic nerves via gp130-signaling cytokines in rodents. *Journal of Clinical Investigation*. **120** (2), 408-421 (2010).
21. Olivas, A. et al. Myocardial infarction causes transient cholinergic transdifferentiation of cardiac sympathetic nerves via gp130. *Journal of Neuroscience*. **36** (2), 479-488 (2016).
22. Yu, L. et al. Optogenetic Modulation of Cardiac Sympathetic Nerve Activity to Prevent Ventricular Arrhythmias. *Journal of the American College of Cardiology*. **70** (22), 2778-2790 (2017).
23. Jungen, C. et al. Increased arrhythmia susceptibility in type 2 diabetic mice related to dysregulation of ventricular sympathetic innervation. *American Journal of Physiology*

- *Heart and Circulatory Physiology*. **317** (6), H1328-H1341 (2019).
24. Hedger, J. H., Webber, R. H. Anatomical study of the cervical sympathetic trunk and ganglia in the albino rat (*Mus norvegicus albinus*). *Acta Anatomica*. **96** (2), 206-217 (1976).
25. Furlan, A. et al. Visceral motor neuron diversity delineates a cellular basis for nipple- and pilo-erection muscle control. *Nature Neuroscience*. **19** (10), 1331-1340 (2016).
26. Al Khafaji, F. A. H., Anderson, P. N., Mitchell, J., Mayor, D. The permeability of the capsule of autonomic ganglia to horseradish peroxidase. *Journal of Anatomy*. **137** (4), 675-682 (1983).
27. Armour, J. A., Murphy, D. A., Yuan, B. X., Macdonald, S., Hopkins, D. A. Gross and microscopic anatomy of the human intrinsic cardiac nervous system. *Anatomical Record*. **247** (2), 289-298 (1997).
28. Fedoroff, S., Richardson, A., Johnson, M. I. Primary Cultures of Sympathetic Ganglia. *Protocols for Neural Cell Culture*. (11051), 71-94 (2003).
29. Scherschel, K. et al. Cardiac glial cells release neurotrophic S100B upon catheter-based treatment of atrial fibrillation. *Science Translational Medicine*. **11** (493), 1-12 (2019).
30. Sun, Y. et al. Sudan black B reduces autofluorescence in murine renal tissue. *Archives of Pathology and Laboratory Medicine*. **135** (10), 1335-1342 (2011).
31. Alanentalo, T. et al. Tomographic molecular imaging and 3D quantification within adult mouse organs. *Nature Methods*. **4** (1), 31-33 (2007).
32. Kersigo, J. et al. A RNAscope whole mount approach that can be combined with immunofluorescence to quantify differential distribution of mRNA. *Cell and Tissue Research*. **374** (2), 251-262 (2018).
33. Schindelin, J. et al. Fiji: An open-source platform for biological-image analysis. *Nature Methods*. **9** (7), 676-682 (2012).
34. Bassil, G. et al. Pulmonary vein ganglia are remodeled in the diabetic heart. *Journal of the American Heart Association*. **7** (23) (2018).
35. Ziegler, K. A. et al. Local sympathetic denervation attenuates myocardial inflammation and improves cardiac function after myocardial infarction in mice. *Cardiovascular Research*. **114** (2), 291-299 (2018).
36. Bayles, R.G. et al. Transcriptomic and neurochemical analysis of the stellate ganglia in mice highlights sex differences. *Scientific Reports*. **8** (1), 8963 (2018).
37. Morales, M.A. et al. Localization of choline acetyltransferase in rat peripheral sympathetic neurons and its coexistence with nitric oxide synthase and neuropeptides. *Proceedings of the National Academy of Sciences of the United States of America*. **92** (25), 11819-11823 (1995).
38. Jimnez, B., Mora-Valladares, E., Zetina, M. E., Morales, M. A. Occurrence, co-occurrence and topographic distribution of choline acetyl transferase, met-enkephalin and neurotensin in the stellate ganglion of the cat. *Synapse*. **43** (3), 163-174 (2002).
39. Ruit, K. G., Osborne, P. A., Schmidt, R. E., Johnson, E. M., Snider, W. D. Nerve growth factor regulates sympathetic ganglion cell morphology and survival in the adult mouse. *Journal of Neuroscience*. **10** (7), 2412-2419 (1990).

40. Guo, J. et al. Involvement of P2Y<sub>12</sub> receptor of stellate ganglion in diabetic cardiovascular autonomic neuropathy. *Purinergic Signalling*. **14** (4), 345-357 (2018).
41. Ajjola, O. A. et al. Remodeling of stellate ganglion neurons after spatially targeted myocardial infarction: Neuropeptide and morphologic changes. *Heart Rhythm*. **12** (5), 1027-1035 (2015).
42. Hinrichs, S. et al. Precursor proadrenomedullin influences cardiomyocyte survival and local inflammation related to myocardial infarction. *Proceedings of the National Academy of Sciences of the United States of America*. **115** (37), E8727-E8736 (2018).
43. Westermann, D. et al. Reduced degradation of the chemokine MCP-3 by matrix metalloproteinase-2 exacerbates myocardial inflammation in experimental viral cardiomyopathy. *Circulation*. **124** (19), 2082-2093 (2011).
44. Johnsen, D., Olivas, A., Lang, B., Silver, J., Habecker, B. Disrupting protein tyrosine phosphatase  $\sigma$  does not prevent sympathetic axonal dieback following myocardial infarction. *Experimental Neurology*. **276**, 1-4 (2016).
45. Manousiouthakis, E., Mendez, M., Garner, M. C., Exertier, P., Makita, T. Venous endothelin guides sympathetic innervation of the developing mouse heart. *Nature Communications*. **5** (May), 3918 (2014).
46. Wink, J. et al. Human adult cardiac autonomic innervation: Controversies in anatomical knowledge and relevance for cardiac neuromodulation. *Autonomic Neuroscience*. **227** (April), 102674 (2020).
47. Kummer, W., Fischer, A., Kurkowski, R., Heym, C. The sensory and sympathetic innervation of guinea-pig lung and trachea as studied by retrograde neuronal tracing and double-labelling immunohistochemistry. *Neuroscience*. **49** (3), 715-737 (1992).
48. Schäfer, M. K. H., Schütz, B., Weihe, E., Eiden, L. E. Target-independent cholinergic differentiation in the rat sympathetic nervous system. *Proceedings of the National Academy of Sciences of the United States of America*. **94** (8), 4149-4154 (1997).
49. Chen, Y. et al. Effect of a Stellate Ganglion block on acute lung injury in septic rats. *Inflammation*. **41** (5), 1601-1609 (2018).
50. Lipov, E. G. et al. Effects of stellate-ganglion block on hot flushes and night awakenings in survivors of breast cancer: a pilot study. *The Lancet Oncology*. **9** (6), 523-532 (2008).
51. Mo, N., Wallis, D. I., Watson, A. Properties of putative cardiac and non-cardiac neurones in the rat stellate ganglion. *Journal of the Autonomic Nervous System*. **47** (1-2), 7-22 (1994).
52. Rajendran, P. S. et al. Identification of peripheral neural circuits that regulate heart rate using optogenetic and viral vector strategies. *Nature Communications*. **10** (1), 1-13 (2019).
53. Hanani, M. Satellite glial cells in sympathetic and parasympathetic ganglia: In search of function. *Brain Research Reviews*. **64** (2), 304-327 (2010).
54. Larsen, H. E., Lefkimiatis, K., Paterson, D. J. Sympathetic neurons are a powerful driver of myocyte function in cardiovascular disease. *Scientific Reports*. **6**, 1-11 (2016).
55. Hasan, W. et al. Sympathetic hyperinnervation and inflammatory cell NGF synthesis following myocardial

infarction in rats. *Brain Research*. **1124** (1), 142-154 (2006).

56. Lorentz, C. U. et al. Heterogeneous ventricular sympathetic innervation, altered  $\beta$ -adrenergic receptor expression, and rhythm instability in mice lacking the p75 neurotrophin receptor. *American Journal of Physiology - Heart and Circulatory Physiology*. **298** (6), 1652-1660 (2010).